

# Two-Phase Flow Modeling of Sediment Motion in Sheet-Flows above Plane Beds

Sandro Longo\*

**Abstract:** Most models of sediment transport are based on the hypothesis of a weak interaction between the fluid and the sediment phase, where the main flow is subjected to the mass and momentum conservation of the fluid phase, with small corrections due to the presence of the sediments. These models usually give a correct answer for conditions where the concentration of sediment is really low. In the case of high sediment transport, some models analyze the two subdomains separately, the high and the low concentration, and employ different constitutive equations. In the present model there is a two-phase description of the whole domain. The closure of the turbulence and the interaction between the sediments and the fluid introduce approximations, but results are consistent with experiments and previous models.

**DOI:** 10.1061/(ASCE)0733-9429(2005)131:5(366)

**CE Database subject headings:** Sediment transport; Sheet flow; Two-phase flow; Granular materials.

## Introduction

Sediment transport in a sheet flow regime occurs in many physical conditions. The field covers a wide range of physical situations: debris flow in its different stages, sheet flow under waves, rivers during flood, or in the swash zone during uprush and down-rush, strong currents and waves, and currents over a plane bed. The importance of such a mechanism of sediment transport is due to the large transport rate relative to all other mechanisms.

The sheet flow regime is characterized by the absence of bed forms, with several layers of grain moving at the bottom at a high volume concentration. Many writers have explored the motion of dry grains in simple bounded flow fields or in unbounded domains, as over an inclined bed (Johnson et al. 1990; Anderson and Jackson 1992; Nott and Jackson 1992) or chutes. In such a situation, the fluid phase plays a secondary role in defining the flow field. The momentum balance equations for the particulate phase need to be supplied with constitutive equations to relate the stress tensor to the state variables and their gradients. The closure is often obtained using the results of the dense gas theory (Lun et al. 1984) for kinetic and collisional stresses, and using the Coulomb approach for the frictional components. A specific effort has been devoted to defining the proper boundary conditions (Haff 1983; Hui et al. 1984; Jenkins and Richman 1986; Pasquarell and Ackermann 1989; Jenkins and Askari 1991; Gutt and Haff 1992), which are extremely important for the modeling of the analytical problem and strengthening the reality of the results.

When the fluid phase plays a significant role in sharing the stresses with the sediment phase, there is the necessity for a

proper modeling of the stress tensors in both phases, including the interactions. The pioneering work of Bagnold (1954) in this direction has been followed by other writers, such as Hanes and Bowen (1985); Ahilan and Sleath (1987); Lamberti et al. (1991); Ribberink and Al Salem (1995); and Dong and Zhang (1999). Detailed experiments are scarce because it is difficult to make accurate measurements in the area of intense sediment transport (Pugh and Wilson 1999). The measure of grain volume concentration requires nonstandard techniques and the use of instruments with strongly nonlinear behavior [Sumer et al. (1996) used inductive probes, Pugh and Wilson (1999) used a  $\gamma$ -ray concentration measuring device].

Considering a stream of water flowing on a bottom with grains, we can expect the following scenarios depending on bottom friction.

1. Fluid stream carrying grains in suspensions at low concentrations. The dynamics of the mixture are similar to the dynamics of the clear water and weakly influenced by the grains. The interactions between grains and mean flow field are represented by drag and lift forces and by the inertia of the added mass. The presence of grains usually reduce the fluid turbulence energy, as low concentration of small particles reduce the resistance of the fluid stream. The interaction between fluid turbulence and grains is different at different wave numbers. At length scales smaller than the grain diameter, the vortices exert a pressure on the grain surface, inducing a random walk of the particle, with a net movement toward regions of less anisotropy in cases of nonisotropic turbulence. At length scales greater than the grain diameter, the grain can be trapped in the vortex motion, provided that the velocity in the vortex is of the order of the settling velocity of the particle. The turbulent field modifications due to grains are mainly restricted to wave numbers larger than the grain wave number (based on grain diameter) in the first case, and are negligible in the second. The grains have negligible self-interactions, but they are quite effective in transferring momentum moving in the flow field. The net flux of momentum, equivalent to a stress, usually acts to equalize the momentum in the flow field.

\*Researcher, Dept. of Civil Engineering, Univ. of Parma, Parco Area delle Scienze, 181/A 43100 Parma, Italy.

Note. Discussion open until October 1, 2005. Separate discussions must be submitted for individual papers. To extend the closing date by one month, a written request must be filed with the ASCE Managing Editor. The manuscript for this paper was submitted for review and possible publication on January 23, 2003; approved on August 31, 2004. This paper is part of the *Journal of Hydraulic Engineering*, Vol. 131, No. 5, May 1, 2005. ©ASCE, ISSN 0733-9429/2005/5-366-379/\$25.00.

2. At intermediate grain volume concentrations, collision between particles is frequent. The granular phase starts to have an independent and significant role in the transmission of stress through collisions, and to transfer energy into pure thermodynamic energy due to inelastic collisions between grains. The fluid acts in reducing the velocity fluctuation of particles, and the scale of the microvortices is strongly damped by the interparticles voids geometry. Fluid jets originate near colliding particles, transferring energy at a length scale smaller than the grain diameter scale. Thus the grains partly act as an energy bypass from the mean motion to the small scale of turbulence.
3. At high grain volume concentration the fluid turbulence energy level decays very fast, and grains carry most of the stress. Using Bagnold's expression for granular stress in inertial regime, we can estimate the order of magnitude of the ratio between the granular stress and the fluid turbulence stress level as

$$\frac{\tau_s}{\tau_f} = O\left(\frac{\rho_s \lambda^2 d^2 (\partial U / \partial y)^2}{\rho_f \mu^2 (\partial U / \partial y)^2}\right) \cong O\left(\frac{\rho_s \lambda^2 d^2}{\rho_f \mu^2}\right) \quad (1)$$

with  $\lambda d$  representing the free path of the grains having diameter  $d$ , and  $l$ =length scale of turbulence.  $O(\dots)$  indicates an order of magnitude [however, Chen and Ling (1996, 1998); and Hunt et al. (2002) revisited Bagnold's data and concluded that the value of the fluid index, the exponent of the shear rate in the constitutive equation, is  $\sim 1.5$ ]. The grains are at contact for a time interval of the order of the time between encounters, the kinetic stress component is negligible, and the quasi-static (friction) stress component tends to dominate the collisional component.

4. For concentrations higher than  $\sim 0.9 C_*$ , where  $C_*$ =maximum packing concentration, the grains state is at rest and the fluid flow field reduces to seepage.

In the present analysis, sediment transport in sheet flow conditions in a general framework is treated. Application is limited to a 1-DV (one dimension in the vertical) formulation. It is assumed that the Shields parameter is high enough ( $\sim 20$  times that required to set individual grains in motion) to prevent bed forms growing and to guarantee the existence of a flat bottom. A two-phase scheme is used in which the two phases, solid and fluid, are considered continua that are mechanically interacting and highly dispersed.

The current paper is organized as follows: a section is dedicated to the governing equations, developed within the general framework of multiphase systems; equations are then written in explicit form for a two-phase system in a 1-DV formulation; closure schemes for turbulence energy and dissipation, and the interaction between the two phases, are outlined in the third and fourth sections; the fifth and sixth sections deal with the rheology of the granular phase and with the boundary conditions for the set of differential equations; the theoretical approach is followed by numerical integration and comparison with experiments or previous models. Comparisons throughout refer to the thickness of the sheet flow layer, to velocity profiles, transport rate, and the friction factor.

## Governing Equations

Considering a multiphase system, the continuity and momentum equations, written in conservative form for the generic phase, are

$$\frac{\partial \rho}{\partial t} + \nabla \cdot (\rho \mathbf{U}) = 0 \quad (2)$$

$$\frac{\partial (\rho \mathbf{U})}{\partial t} + \nabla \cdot (\rho \mathbf{U} \mathbf{U}) + \nabla \cdot \mathbf{T} - \rho \mathbf{f} = 0 \quad (3)$$

$$T_{ij} = T_{ji}$$

where  $\rho$ =mass density;  $\mathbf{U}$ =velocity; and  $\mathbf{U}\mathbf{U}=U_n \otimes U_m$ =tensorial product of the two vectors  $\mathbf{U}$ ;  $\mathbf{T}$ =stress tensor; and  $\mathbf{f}$ =force per unit mass. All the variables are local and instantaneous. To avoid solving a multiboundary problem, and to remove the fluctuations of the variables, we adopt Reynolds decomposition and a space average as suggested by Drew (1983). Following Drew (1983), we introduce the phasic function  $X_j(\mathbf{x}, t)=1$  if the vector position  $\mathbf{x}$  is in the phase  $j$  at the time  $t$ , otherwise  $X_j(\mathbf{x}, t)=0$ . Considering any tensor  $h$  function of space  $\mathbf{x}$  and time  $t$  and a weighting function  $a(\mathbf{s})$ , where  $\mathbf{s}$ =space vector describing the volume of integration  $V$ , its space average is  $\langle h \rangle = \int_V h(\mathbf{x} + \mathbf{s}, t) a(\mathbf{s}) dV$ . Multiplying the mass and the momentum conservation equations by the generalized function  $X_j$  and averaging in space, yields

$$\frac{\partial \Phi_j \tilde{\rho}_j}{\partial t} + \nabla \cdot (\Phi_j \tilde{\rho}_j \hat{\mathbf{U}}_j) = 0 \quad (4)$$

$$\frac{\partial (\Phi_j \tilde{\rho}_j \hat{\mathbf{U}}_j)}{\partial t} + \nabla \cdot (\Phi_j \tilde{\rho}_j \mathbf{U}_j \hat{\mathbf{U}}_j) = - \nabla \cdot (\Phi_j \tilde{\mathbf{T}}_j) + \Phi_j \tilde{\rho}_j \hat{\mathbf{f}}_j + \mathbf{M}_j \quad (5)$$

where  $\Phi_j = \langle X_j \rangle$ ;  $\mathbf{M}_j = \langle \mathbf{T}^j \cdot \nabla X_j \rangle$ =interfacial force ( $\nabla X_j$  is nonzero only at the interface between the two phases) and the symbols

$\langle \dots \rangle = \langle X_j(\dots) \rangle / \langle X_j \rangle = \langle X_j(\dots) \rangle / \Phi_j$ ;  $\langle \dots \rangle = \langle X_j \rho(\dots) \rangle / \langle X_j \rho \rangle$ =phasic and density weighted average operators. We have assumed no phase change, and we have neglected the mass and the stresses at the interface. If the fluid phase behaves like a Newtonian fluid, the stress tensor  $\tilde{\mathbf{T}}_f$  is decomposed in terms of pressure and extra stresses

$$\tilde{\mathbf{T}}_f = (\tilde{p}_f - \lambda_f \tilde{\nabla} \cdot \mathbf{U}_j) \mathbf{I} - 2\mu_f \tilde{\mathbf{D}}_f \quad (6)$$

where  $\tilde{p}_f$ =isotropic component of  $\tilde{\mathbf{T}}_f$ ;  $\mathbf{D}_f$ =rate of deformation tensor; and  $\lambda_f$  and  $\mu_f$ =bulk and shear viscosities, which are assumed constant and uniform.

The stress tensor in the granular phase can be similarly expressed, with bulk and shear viscosities and isotropic pressure dependent on the grain volume concentration and pseudotemperature (pseudotemperature is the variance of the grain velocity, equivalent to kinetic turbulent energy for the fluid phase). If the pseudotemperature is treated as an independent variable, the structure of Eq. (6) is also formally correct for the granular phase.

We assume that the interface term  $\mathbf{M}_j$  can be decomposed as follows:

$$\mathbf{M}_j = p_{j,\text{int}}^j \nabla \Phi_j + \mathbf{M}_j^d \quad (7)$$

where  $p_{j,\text{int}}^j$ =interfacial pressure on the  $j$  side and  $\mathbf{M}_j^d = \langle (p - p_{j,\text{int}}) \nabla X_j \rangle - \langle \tau_j^j \cdot \nabla X_j \rangle$ =interfacial force density. For a constant interfacial pressure  $p_{j,\text{int}}^j$  over a particle scale, the equality  $\langle p_{j,\text{int}}^j \nabla X_j \rangle = p_{j,\text{int}}^j \nabla \Phi_j$  holds.

For a two-phase system the number of unknowns is greater than the number of equations, and assumptions of closure are

needed to relate the stresses  $\bar{\tau}_j$  to the characteristics of the flow field (three equations per phase). To describe the pressure difference ( $p_{j,\text{int}}^j - \bar{p}_j$ ) for each phase and the interfacial force density  $\mathbf{M}_j^d$ , a relation is required between the isotropic pressures of the two phases, between the variables  $\Phi_j$ , in terms of the state variables. We will assume that both phases are incompressible,  $\bar{\rho}_j = \text{const}$ , and that  $\Phi_s = C$  and  $\Phi_f = 1 - C$ . We also introduce Reynolds decomposition of the instantaneous space and time averaged variables.

In uniform conditions, variation in the  $x$  direction is zero and only variation in the  $y$  direction is important. For fluid-particle mixtures in a 2D system, the equations of continuity and linear momentum balance in 1-DV formulation reduce to

$$\rho_f \frac{\partial(1-C)U_x}{\partial t} + \rho_f \frac{\partial(1-C)U_x U_y - \overline{C'U'_y U_x}}{\partial y} + (1-C) \frac{\partial p}{\partial x} + \rho_f \frac{\partial(1-C)\overline{U'_x U'_y}}{\partial y} - \rho_f(1-C)g \sin \alpha + M_{sx}^d = 0 \quad (8)$$

$$\rho_s \frac{\partial C V_x}{\partial t} + \rho_s \frac{\partial C V_x V_y + \overline{C'V'_y V_x}}{\partial y} + C \frac{\partial p}{\partial x} + \frac{\partial(\tau_{sc} + \rho_s \overline{C'V'_x V'_y})}{\partial x} - \rho_s C g \sin \alpha - M_{sx}^d = 0 \quad (9)$$

$$\rho_f \frac{\partial(1-C)U_y - \overline{C'U'_y}}{\partial t} + \rho_f \frac{\partial(1-C)U_y U_y - 2\overline{C'U'_y U_y}}{\partial y} + (1-C) \frac{\partial p}{\partial y} + \rho_f \frac{\partial(1-C)\overline{U'_y U'_y}}{\partial y} + \rho_f(1-C)g \cos \alpha + M_{sy}^d = 0 \quad (10)$$

$$\rho_s \frac{\partial C V_y + \overline{C'V'_y}}{\partial t} + \rho_s \underbrace{\frac{\partial C V_y V_y + 2\overline{C'V'_y V_y}}{\partial y}}_I + C \underbrace{\frac{\partial p}{\partial y}}_{II} + \underbrace{\frac{\partial(\sigma_{sc} + \rho_s \overline{C'V'_y V'_y})}{\partial y}}_{III} + \underbrace{\rho_s C g \cos \alpha}_{IV} - \underbrace{M_{sy}^d}_{Va, Vb} = 0 \quad (11)$$

$$-\frac{\partial C}{\partial t} + \frac{\partial(1-C)U_y - \overline{C'U'_y}}{\partial y} = 0 \quad (12)$$

$$\frac{\partial C}{\partial t} + \frac{\partial C V_y + \overline{C'V'_y}}{\partial y} = 0 \quad (13)$$

with  $\mathbf{U} \equiv (U_x, U_y)$  and  $\mathbf{V} \equiv (V_x, V_y)$  being the fluid and sediment velocity. All the variables are time averaged, and the overbar indicates the time correlation. The viscous contribution in the carrier phase is neglected as it is of a small order. It is assumed that the interface effects are negligible, and the isotropic pressure in the fluid and granular phase is in equilibrium, with  $p_{f,\text{int}}^f = p_{s,\text{int}}^s \equiv p_{\text{int}} = p_f = p_s$ . The time derivatives are retained only for numerical purpose, as explained in ‘‘Application.’’

## Closure Scheme and Interaction between the Two Phases

In the set of equations [(8)–(13)] more unknowns than equations are still present. We need constitutive relations to model

$\overline{U'_i U'_j}, \overline{C'U'_i}, \overline{C'V'_i}, \mathbf{M}_s^d, \mathbf{M}_f^d$ . The correlations between the fluctuating terms of the fluid velocity can be modeled using a diffusive scheme

$$\overline{U'_i U'_j} = -v_t(U_{i,j} + U_{j,i}) + \frac{2}{3}\delta_{ij}\kappa - \frac{2}{3}v_t\delta_{ij}U_{j,j} \quad (14)$$

$$\overline{C'U'_i} = \overline{C'V'_i} = -\frac{v_t}{\text{Sc}_c}C_i$$

with  $v_t = C_\mu(\kappa^2/\varepsilon)$ ,  $\kappa = \frac{1}{2}\overline{U'_i U'_i}$ , and  $\text{Sc}_c$  denoting the turbulent Schmidt’s number for concentration. The pressure-concentration correlations have been dropped for simplicity, even though they could be modeled using previously published schemes (e.g., Rotta 1951).

The components of the interfacial force density,  $\mathbf{M}_f^d$ ,  $\mathbf{M}_s^d$  and their fluctuations, can be specified on the basis of the force acting on an insulated moving sphere in a generic flow. The hydrodynamic force acting on the granular phase is expressed as

$$\mathbf{M}_s^d = n\mathbf{F} = \rho_f C \left[ \frac{3}{4}C_{De} \frac{1}{d} |\mathbf{U} - \mathbf{V}| (\mathbf{U} - \mathbf{V}) + C_{Me} \left( \frac{D_f \mathbf{U}}{Dt} - \frac{D_s \mathbf{V}}{Dt} \right) + C_{Le} (\mathbf{U} - \mathbf{V}) \wedge \boldsymbol{\Omega} \right] \quad (15)$$

with  $n = 6C/\pi d^3$  representing the number of particles per unit volume. The coefficients  $C_{De}$ ,  $C_{Me}$ , and  $C_{Le}$  = effective drag, adjoint-mass, and lift coefficients evaluated for a cloud of particles, respectively. The term representing pressure effects is already present in the linear momentum balance equation, and has been dropped in the expression of the interfacial momentum transfer.  $\boldsymbol{\Omega}$  = vorticity, and  $D_s$  and  $D_f$  = material derivative following the sediments and the fluid, respectively. The lift term is not widely used also because it is difficult to measure. In addition it is questionable to introduce it if the particle is of the same size of the smallest wavelength of the turbulence (Tchen 1947).

A Reynolds decomposition of the interfacial momentum transfer generates 14 new components involving correlations. These components have not been further analyzed due to the difficulty in modeling and validating all of their correlations.

Experimental relationships are available for the effective drag coefficients (Rubey 1933; Maude and Whitmore 1958)

$$C_{De} = \left( \frac{24}{R_d} + 2 \right) / (1-C)^{4.5}; \quad R_d = \frac{|\mathbf{U} - \mathbf{V}|d}{\nu} \quad (16)$$

A semiempirical correction for the added mass coefficient, valid to the order  $O(C)$  obtained by Mokeyev (1977), is represented by the equation  $C_{Me} = C_M(1 + 4.2C)$ , where  $C_M = 0.5$ . Unfortunately, similar equations are not available that include the effect of a cloud of particles in the residual coefficients. For the lift we assume that  $C_{Le} = C_L = 0.5$ .

The force densities  $\mathbf{M}_f^d$  for the two phases have to be equal and with opposite sign, with  $\mathbf{M}_f^d = -\mathbf{M}_s^d$ .

## Closure of the Turbulence Energy Equation

Modeling turbulence in a two-phase system is more complicated than in a single phase, with fluid turbulence being strongly influenced by the motion of the grains. We adopt a classical  $\kappa$ - $\varepsilon$  model, modified to include extra-production and extra-dissipation

terms due to the presence of sediments, as proposed by Elghobashi and Abou-Arab (1983). The modeled equation for turbulent kinetic energy is represented as follows:

$$\begin{aligned} & \rho_f(1-C)\frac{\partial k}{\partial t} + \rho_f(1-C)U_y\frac{\partial k}{\partial y} - 2\rho_f\frac{v_t}{Sc_k}k\frac{\partial^2 C}{\partial y^2} \\ & + \rho_f C_{Me}C(V_y - U_y)\frac{\partial k}{\partial y} \\ & = \underbrace{\rho_f\frac{\partial[(1-C)v_t\partial k/\partial y]}{\partial y}}_D + \underbrace{\rho_f(1-C)v_t\left(\frac{\partial U_x}{\partial y}\right)^2}_P \\ & - \underbrace{\frac{v_t}{Sc_c}\frac{\partial C}{\partial y}\frac{\partial p}{\partial y}}_{P_{extra}} - \rho_f(1-C)\varepsilon - \underbrace{\frac{F_{stat}}{|V_y - U_y|} \frac{v_t}{Sc_c}\frac{\partial C}{\partial y}(V_y - U_y)}_{\varepsilon_{extra}} \\ & F_{stat} = \rho_f C \left( \frac{3}{4} C_{De} \frac{1}{d} |\mathbf{U} - \mathbf{V}|^2 + C_{Le} |(\mathbf{U} - \mathbf{V}) \wedge \Omega| \right) \quad (17) \end{aligned}$$

where  $\kappa = 0.5 \overline{U'_i U'_i}$  represents the fluid turbulent kinetic energy; and  $\varepsilon = \nu \overline{U'_{i,k} U'_{i,k}}$  is its rate of dissipation,  $Sc_\kappa$  is the Schmidt's number for turbulence energy,  $F_{stat}$  is part of the stationary drag. The terms on the left-hand side of the equation model transient and convection effects; the terms on the right-hand side represent turbulent diffusion ( $D$ ), production ( $P$ ), extra production due to buoyancy ( $P_{extra}$ ), dissipation, and extra dissipation ( $\varepsilon_{extra}$ ).

A similar equation can be obtained for the turbulence energy dissipation:

$$\begin{aligned} & \rho_f(1-C)\frac{\partial \varepsilon}{\partial t} + \rho_f(1-C)U_y\frac{\partial \varepsilon}{\partial y} - 2\rho_f\varepsilon\frac{v_t}{Sc_c}\frac{\partial^2 C}{\partial y^2} \\ & = -\rho_f\frac{\partial\left((1-C)(v_t/Sc_c)\frac{\partial\varepsilon}{\partial y}\right)}{\partial y} \\ & + C_{\varepsilon 1}(P + P_{extra})\frac{\varepsilon}{k} + \rho_f(1-C)(C_{\varepsilon 2}\varepsilon + C_{\varepsilon 3}\varepsilon_{extra})\frac{\varepsilon}{k} \quad (18) \end{aligned}$$

where  $Sc_\varepsilon$ =Schmidt's number for turbulence energy dissipation. The model involves a few coefficients whose values have been set on the basis of computer simulation or experimental evidence. The assumed values of the coefficients are reported in Table 1 and are commonly used in literature (e.g., Elghobashi and Abou-Arab 1983). There are some theoretical difficulties with evaluating the rate of dissipation  $\varepsilon$  in dense particle flows. The rate of dissipation is usually related to the length scale of the vortices most effective in dissipation,  $\varepsilon \propto k^{3/2}/L$ . In dense-particle flows the scale of these vortices can be limited by the interparticle distance. To include this effect, Kenning and Crowe (1997) introduced a hybrid length scale for viscous dissipation which depends on both the average interparticle spacing and the dissipation scale of the fluid in the absence of particle.

## Stress Tensor in the Granular Phase

The sediment kinetic and collisional stresses are modeled according to Lun et al. (1984). The writers modify the theory of dense gases of Chapman and Cowling (1970) to account for the elasticity of grains, and express the transport coefficients as function of (1) a pseudotemperature  $T \propto |\mathbf{V}'|^2$  (it corresponds to fluid turbulence energy), (2) the local concentration, and (3) the restitution

**Table 1.** Value Adopted for the Coefficients in  $\kappa$ - $\varepsilon$  Turbulence Model (from Elghobashi and Abou-Arab 1983)

Coefficient	Value adopted in the present model
$C_\mu$	0.09
$C_{\varepsilon 1}$	1.44
$C_{\varepsilon 2}$	1.92
$C_{\varepsilon 3}$	1.2
$Sc_\varepsilon$	1.3
$Sc_\kappa$	1.0
$Sc_c$	1.0

coefficient. Pseudothermal energy is generated, convected, diffused, and dissipated according to a balance equation. The main mechanisms of transmission of stresses are binary collisions between particles (collisional component) and flux of momentum (kinetic component). The model neglects particle rotation and the interparticle fluid.

Among all the micromechanics theories, the model by Lun et al. (1984) covers the entire range of concentrations and has been tested widely against other similar models and experimental results of dry grains motion over inclined beds and chutes (e.g., Nott and Jackson 1992).

In compact form, the kinetic and collisional stresses in the granular phase are represented by

$$\begin{aligned} \sigma_{sk} + \sigma_{sc} &= \rho_s f_1 T - \chi \left( f_{11} - \frac{f_2}{2} \right) \sqrt{T} \left( \frac{\partial V_y}{\partial y} \right) \\ \tau_{sk} + \tau_{sc} &= -\chi \frac{f_2}{2} \sqrt{T} \left( \frac{\partial V_x}{\partial y} \right) \end{aligned} \quad (19)$$

where  $f_1$ ,  $f_{11}$ , and  $f_2$ =functions of the concentration, the maximum concentration  $C_*$ , and the coefficient of elasticity of the spherical particles. The variable  $\chi$  depends on grain mass volume and diameter.

The balance equation for the pseudothermal energy is

$$\begin{aligned} & \frac{3}{2}\rho_s C \left( \frac{\partial T}{\partial t} + V_y \frac{\partial T}{\partial y} \right) + \frac{\partial q_{PTy}}{\partial y} + (\sigma_{sk} + \sigma_{sc}) \frac{\partial V_y}{\partial y} + (\tau_{sk} + \tau_{sc}) \frac{\partial V_x}{\partial y} + I \\ & = 0 \end{aligned} \quad (20)$$

where  $q_{PTy}$ =vertical component of the pseudothermal flux

$$q_{PTy} = -\lambda f_3 \frac{\partial T}{\partial y} \sqrt{T} - \lambda f_4 \frac{\partial C}{\partial y} T \sqrt{T} \quad (21)$$

and  $I$ =dissipation rate

$$I = \frac{\rho_s}{d} f_5 T \sqrt{T} \quad (22)$$

where  $f_3$ ,  $f_4$ , and  $f_5$ =functions of the concentration, the maximum concentration  $C_*$ , and the coefficient of elasticity of the spherical particles. The variable  $\lambda$  depends on grain mass volume, grain diameter, and elastic restitution coefficient.

The value of the restitution coefficient should be related to the interparticle fluid, to the shape of the particles and the roughness of their surface, and to the relative velocity of impact. Different values of the elastic restitution coefficients between particles in the shear layer ( $e$ ) and between particles in motion and a particle at rest representing the boundary ( $e_w$ ), reflect the different dynamics of collisions.

At high volume concentrations, another source of stress is friction. The available models for frictional stresses are less sophisticated, and mainly empirical. In fully developed plane shearing, a simple relationship between frictional normal stress and concentration is provided by Johnson and Jackson (1987)

$$\sigma_{fric} = \frac{F_s}{(C_0 - C)^n} \quad (23)$$

where the exponent  $n$  is very high (of the order of 40), and  $F_s$ =coefficient of the order  $10^{-30}$  N/m<sup>2</sup>.  $C_0$  is assumed to equal the maximum concentration. Performing the local analysis of equilibrium, the frictional contribution to the shear stress is given by

$$\tau_{fric} = -\sigma_{fric} \tan \varphi_d \quad (24)$$

where  $\varphi_d$ =internal friction angle in dynamic conditions. We also assume that the frictional stresses can simply be added to dispersive stresses.

The last term to be modeled is the component of the gradient pressure parallel to the bottom in the main direction of motion. In general, it is driven by the free stream motion, as represented by

$$\frac{\partial p}{\partial x} = \rho_f \frac{\partial U}{\partial t} - \rho_f g \eta + \rho_f g \sin \alpha \quad (25)$$

where  $U(t)$ =external velocity;  $\eta$ =surface slope to generate the current; and  $\alpha$ =bottom slope angle.

The model has been applied to a case involving a free stream in a uniform steady condition over an inclined mobile bed with a zero pressure gradient in the direction of motion.

## Boundary conditions

The following set of boundary conditions at the bottom ( $y=y_b$ ) and free surface ( $y=y_t$ ) are fixed:

$$\begin{aligned} U_x(y_b) &= u_{seep} \\ V_x(y_b) &= U_y(y_b) = V_y(y_b) = 0 \\ \left( CV_y - \frac{v_t}{Sc_c} \frac{\partial C}{\partial y} \right)_{y=y_t} &= 0 \\ \frac{\partial U_x}{\partial y} \Big|_{y=y_t} &= \frac{\partial V_x}{\partial y} \Big|_{y=y_t} = 0 \\ \frac{\partial \kappa}{\partial y} \Big|_{y=y_t} &= \frac{\partial \varepsilon}{\partial y} \Big|_{y=y_t} = \frac{\partial T}{\partial y} \Big|_{y=y_t} = p(y_t) = 0 \end{aligned} \quad (26)$$

where  $u_{seep}$ =seepage fluid velocity. This value can be set to zero with negligible error.

More detailed boundary conditions at the bottom are necessary for the pseudotemperature, turbulence energy, and dissipation rate concentration. Following Jenkins and Richman (1986), the balance of pseudoenergy at the bottom can be written as

$$-\mathbf{n} \cdot \mathbf{q}_{PT} = D \quad (27)$$

where  $\mathbf{n}$ =outward normal, and  $D$ =rate of dissipation of pseudoenergy due to the particle-boundary collisions as a function of the coefficient of restitution of energy  $e_w$  for collisions between grains in motion and grains at rest. Eq. (27) can be expressed in compact form as

$$f \left( \frac{\partial C}{\partial y}, \frac{\partial T}{\partial y}, C, T \right) = 0 \quad (28)$$

The boundary condition for  $\varepsilon$  and  $\kappa$  at the bottom are fixed in the hypothesis of local balance of production and dissipation of turbulence energy near the bottom. A logarithmic velocity profile, coupled with a consideration of the influence of the sediments through the Richardson flux number (Brørs 1991), yields

$$\kappa = \frac{4.05 u_*^2}{2 \sqrt{0.19 + \frac{(0.06 - 0.48 Ri)}{(1 - Ri)}}} \quad (29)$$

$$\varepsilon = \frac{u_*^3}{k y} (1 - Ri)$$

where  $u_*$ =friction velocity related to the fluid tangential stress;  $k$ =Von Kármán's constant; and  $Ri$  is the gradient Richardson number. The gradient Richardson number, defined as the ratio between the generation of turbulent energy due to buoyancy and shear, can simply be defined as

$$Ri = \frac{v_t \frac{g(\rho_s - \rho_f)}{Sc_c [\rho_s C + \rho_f(1 - C)]} \frac{\partial C}{\partial y}}{v_t \left( \frac{\partial U_x}{\partial y} \right)^2} \quad (30)$$

It is still necessary to fix the boundary condition for the concentration. The Coulombic equilibrium for the first layer of grains at rest below flowing sediments is

$$|\tau_s| \leq |\sigma_{sc} + \sigma_{sk} + \sigma_{fric}| \tan \varphi_s \quad (31)$$

where  $\varphi_s$ =internal friction angle in static condition.

Using Eqs. (23) and (24), Eq. (31) is arranged as

$$C_b = C_0 - n \sqrt{\frac{F_s \tan \varphi_s}{|\tau_s| - |\sigma_{sc}| \tan \varphi_s}} \quad (32)$$

It is a limiting condition. The minimum concentration at the bottom is a function of the stresses near the bottom. The bottom concentration is slightly less than the reference concentration, and higher values of the friction static internal angle require smaller bottom concentration. The kinetic contribution  $\sigma_{sk}$  is negligible at high concentration.

## Application

The differential problem contains nine partial differential equations, i.e., two linear momentum balance equations in the horizontal [Eqs. (8) and (9)], two linear momentum balance equations in the vertical [Eqs. (10) and (11)], two equations of continuity [Eqs. (12) and (13)], turbulence energy and turbulence energy dissipation balance [Eqs. (17) and (18)], and the pseudoenergy balance [Eq. (20)] with nine unknowns: two horizontal and two vertical velocities for fluid and grains, fluid pressure, grain volume concentration, turbulence energy and turbulence dissipation, and pseudotemperature. The integration of the differential problem has been carried out using a time relaxation scheme that is explicit with respect to time, and implicit with respect to space. Only the continuity equation has been integrated using a McCormack predictor-corrector explicit scheme. A stag-

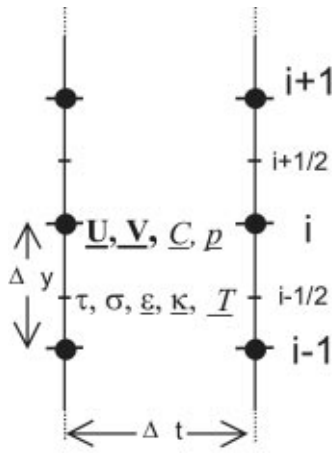


**Fig. 1.** Staggered grid used for the numerical computations

gered nonuniform grid has been used, with the state variables computed at the main and midnode as shown in Fig. 1. The underlined variables represent the unknowns.

The finite-difference scheme leads to a nonlinear system of equations at each time step, reduced to a tridiagonal linearized system. The system is solved utilizing the Thomas algorithm, and time integration is stopped when the nonstationary terms become several orders of magnitude smaller than the other terms. The grid contains 100 nodes with successful tests to check the grid space independence of the scheme. The number of nodes has been fixed to obtain a space step equivalent to the grain diameter near the bottom. The system is strongly nonlinear and generally sensitive to small variations in posing the boundary conditions. The boundary conditions for the turbulent kinetic energy and dissipation and pseudotemperature are applied at the first midnode over the bottom, where the space step is of the order of the grain diameter. Some sensitivity tests on optimal space step showed that the solution is invariant choosing a grid with smaller size but checking that the first midnode over the bottom is in the domain where molecular viscosity has negligible effects.

Comparison has been made with the experiments of Sumer et al. (1996) and of Nnadi and Wilson (1992) with respect to concentration, friction factor, and total sediment load. Sumer et al. (1996) have carried out experiments in a tilting flume with dimensions 0.3 by 0.3 m. Most of the tests were conducted with a lid, while some were conducted with a free surface flow. Four different sediments were used, but we compare some of the results obtained for only two of the sediment types. These are named Nos. 3 and No. 4 in the original paper, and 3a and 4a in the present paper. Properties of these sediments are shown in Table 2. We have supposed a free surface flow, with a depth of 0.08 m for the experiment with sand grains and 0.11 m for the experiments with acrylic grains. The water depth was chosen, jointly with the bottom inclination, in order to obtain a value of the Shields parameter equal to the value listed by Sumer et al. for the correspondent experiments. The depth is not relevant as long as the

**Table 2.** Material Properties (from Sumer et al. 1996)

Sediment	Material	Grain size (m)	Dry relative density	Fall velocity (m/s)	Remarks
3a	Acrylic	$0.60 \times 10^{-3}$	1.13	$2.0 \times 10^{-2}$	Spherical grains with $d_{50} = 0.60 \times 10^{-3}$ m
4a	Sand	$0.13 \times 10^{-3}$	2.65	$1.2 \times 10^{-2}$	Natural sand with $d_{50} = 0.13 \times 10^{-3}$ m

**Table 3.** Material Properties (from Nnadi and Wilson 1992)

Number	Material	Grain size (m)	Dry relative density
1b	Bakelite	$1.05 \times 10^{-3}$	1.56
2b	Bakelite	$0.67 \times 10^{-3}$	1.56
3b	Sand	$0.70 \times 10^{-3}$	2.67
4b	Nylon	$3.94 \times 10^{-3}$	1.14

boundary conditions listed in Eq. (26) are smoothly satisfied. If not, the signals of ill-posedness of the scheme are strong numerical instabilities and consequent crashing of the numerical code. In real systems, some instabilities can develop, but the treatment of these instabilities and their interpretation is beyond the scope of the present work. For the modeled experiments, a limiting lower value of the depth is  $\sim 30\%$  less than the chosen depth of 0.08 and 0.11 m, whereas increasing the chosen depth does not modify the results in the domain of interest.

Nnadi and Wilson (1992) report the results of experiments conducted in a pressurized horizontal conduit of square cross section  $9.8 \times 9.8$  cm. They used four different sediments, as reported in Table 3, measuring discharges of slurry and of solids, depth of flows, and pressure gradients in order to calculate the relevant parameter of the motion. The values for the parameters adopted in the present model are in reported in Table 4.

Fig. 2 displays the main terms for linear momentum balance for sediment phase [Eq. (11)]. The upper limit of the sheet-flow layer is drawn according to the analysis presented in a subsequent section. Convection [term  $I_a$  in Eq. (11)] is of lower order with respect to other contributions, and is not shown. In the suspension domain, the balance is essentially amongst buoyancy (II), gravity (IV), and drag ( $V_a$ ). The intergranular stress gradient (III) and lift ( $V_b$ ) are significant only in the sheet-flow layer. Diffusion ( $I_b$ ) is important at the interface.

Figs. 3 and 4 display the  $\kappa$ - $\varepsilon$  equation balances. Diffusion is negligible and convection is significant only in the sheet-flow layer, and in the suspension domain the balance is local. Turbulence energy and dissipation (see Figs. 5 and 6) reach a maximum in the sheet-flow layer and decay monotonically for sand. The acrylic grains show a slightly different behavior, with lower values for turbulence. Turbulent diffusivity is strongly damped in the grain bed, with a length scale related to the mean distance among the grain particles (Fig. 7).

Figs. 8 and 9 display the pseudothermal energy balance and the pseudotemperature distribution. The balance tends to be local only near the top of the sheet-flow layer, where the pseudotemperature is a minimum.

### Thickness of the Sheet-Flow Layer

The sheet-flow layer is usually defined as a region of the domain where the grains are supported mainly by intergranular stress due to collision. The momentum exchange due to transfer of particles

**Table 4.** Material Properties Adopted in the Present Model

Property	Acrylic	Sand
$d$	$0.60 \times 10^{-3}$ m	$0.13 \times 10^{-3}$ m
$e$	0.8	0.8
$e_w$	0.6	0.6
$F_s$	$3.6 \times 10^{-31}$ Pa	$3.6 \times 10^{-31}$ Pa
$n$	40	40
$\varphi_s$	$26^\circ$	$32^\circ$
$\varphi_d$	$25^\circ$	$31^\circ$
$\rho_s$	$1,130 \text{ kg m}^{-3}$	$2,650 \text{ kg m}^{-3}$

between regions with different mean velocities can be neglected in this layer. A number of expressions for sheet-flow layer thickness can be found in the literature. Following Hanes and Bowen (1985) (hereafter HB) and assuming a hydrostatic fluid pressure, a linear concentration profile, and a constant dynamic friction angle, the relative thickness of the sheet-flow layer may be expressed as

$$\frac{\delta}{d} = \frac{2\Theta(1/\tan \varphi_r - 1/\tan \varphi_d)}{C_0 + C_\delta} \quad (33)$$

where  $\varphi_r$ =critical dynamic angle of internal friction;  $\varphi_d$ =dynamic friction angle; and  $C_\delta$ =grain volume concentration at the top of the layer.

Kobayashi and Seo (1985) (hereafter KS) locate the interface between the bed load and the suspended load regions at a relative height with the expression

$$\frac{\delta}{d} = \sqrt{\frac{\Theta}{\Theta_c}} \quad (34)$$

where  $\Theta_c$ =critical Shields parameter, whose value is a function of the Reynolds particle number and asymptotically equal to 0.06.

Wilson (1987) and Wilson and Pugh (1988) (hereafter WP) utilize the following expression:

$$\frac{\delta}{d} = \frac{\Theta}{\bar{C} \tan \varphi} \quad (35)$$

where  $\varphi'$ =Coulombic friction angle; and  $\bar{C}$ =mean concentration in the layer. Pugh and Wilson (1999) performed detailed experiments to measure a linear concentration profile near the bottom,

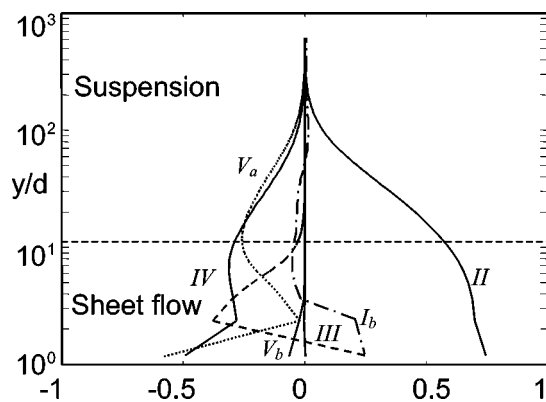


**Fig. 2.** Balance among the different terms of Eq. (11) in stationary conditions.  $d=0.13$  mm,  $s=2.65$ , and  $\Theta=1.68$

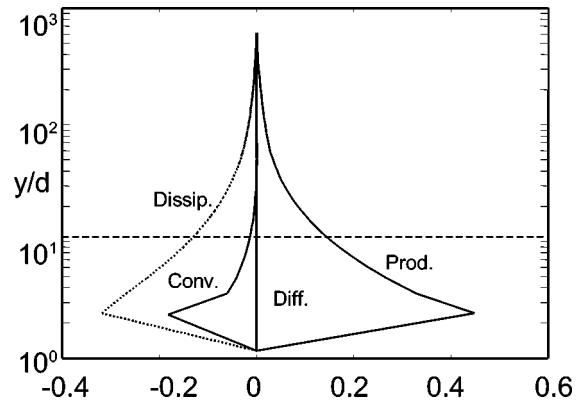


**Fig. 3.**  $\kappa$ -equation balance.  $d=0.13$  mm,  $s=2.65$ , and  $\Theta=1.68$

and used this feature to define the layer height. The top-level concentration on average is equal to  $\sim 0.05$ .

Sumer et al. (1996) evaluated the thickness of the sheet-flow layer from concentration profile measurements for acrylic 0.6 mm and from visual observations for plastic (3.0 and 2.6 mm). The prediction from the concentration measurements is the largest, probably because strong errors are implicit in this method.

A criterion suggested here consists of relating the thickness of the sheet-flow layer to the stress regime. An initial definition is based on the following considerations. Fluid tangential stress decays near the bottom, where sediment tangential stress becomes dominant. The top level of the sheet-flow layer can be assumed to correspond to the inflexion point of the fluid tangential stress profile, where a negligible grain stress is present as shown in Fig. 10. A second definition is based on the ratio between fluid tangential stress and sediment tangential stress. We can assume the sheet-flow layer extends to the domain where fluid tangential stress becomes  $< 1\%$  of the sediment tangential stress.

The results of numerical simulations are compared to the WP layer height and to the HB sheet-flow thickness, with a top-layer concentration of 0.05 and a critical friction angle of  $31$  and  $25^\circ$  for sand and acrylic, respectively, and to KS sheet-flow thickness with  $\Theta_c=0.06$ . The definition based on the inflexion point of the fluid tangential stress shows that the values for sand and acrylic tend to be unique for high Shields parameters, with relative thickness being higher for sand than for acrylic. The computed thickness is much smaller than the measured thickness based on the criterion of Pugh and Wilson (1999), as indicated in Fig. 11(a).

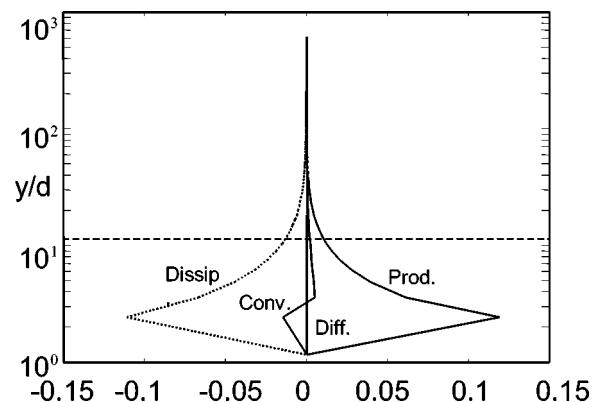


**Fig. 4.**  $\epsilon$ -equation balance.  $d=0.13$  mm,  $s=2.65$ , and  $\Theta=1.68$

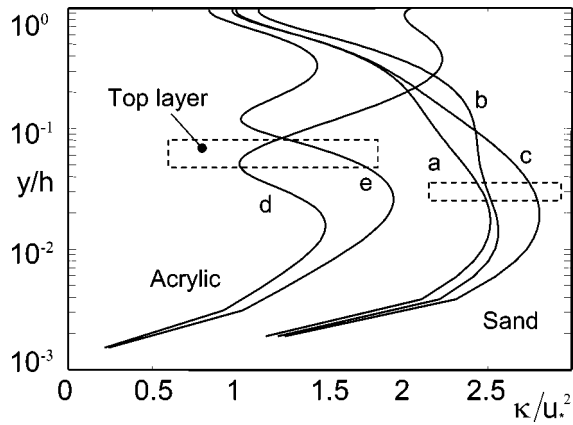


Fig. 5. Turbulence energy distribution, see Table 5 for caption

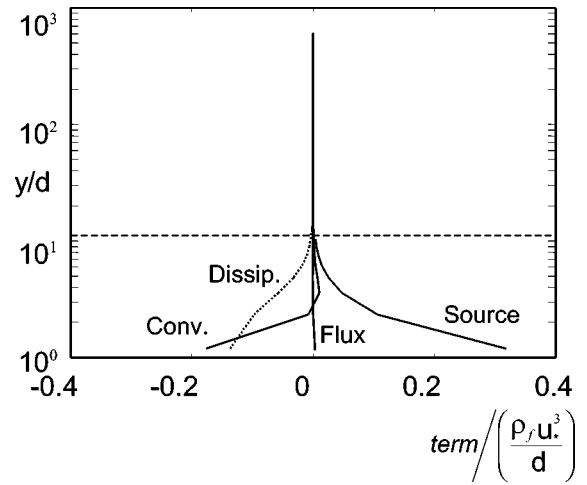


Fig. 8. Pseudothermal energy balance

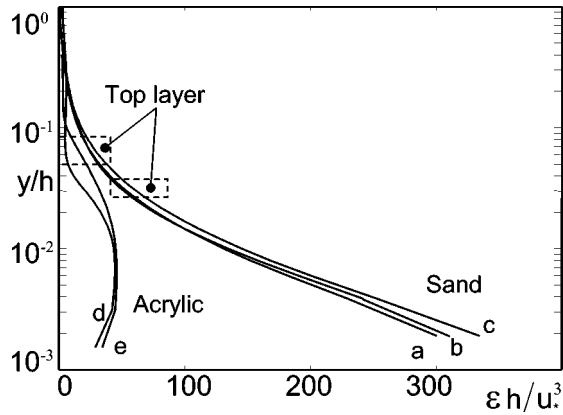


Fig. 6. Turbulence dissipation, see Table 5 for caption

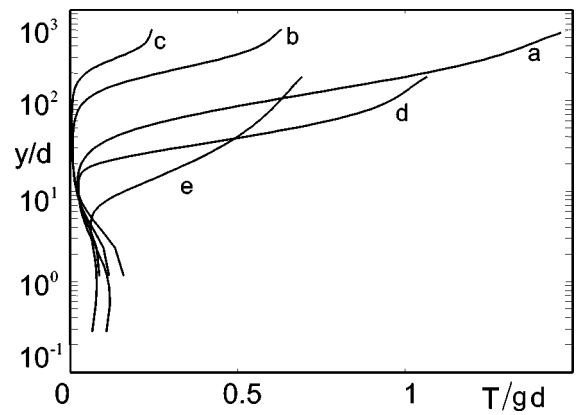


Fig. 9. Pseudotemperature distribution, see Table 5 for caption

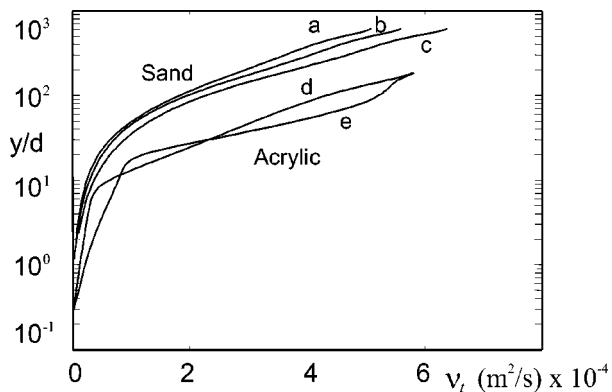


Fig. 7. Turbulent diffusivity, see Table 5 for caption

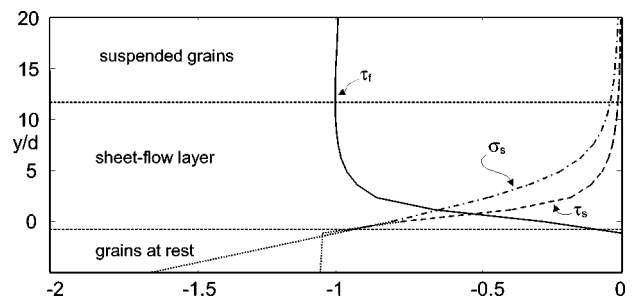
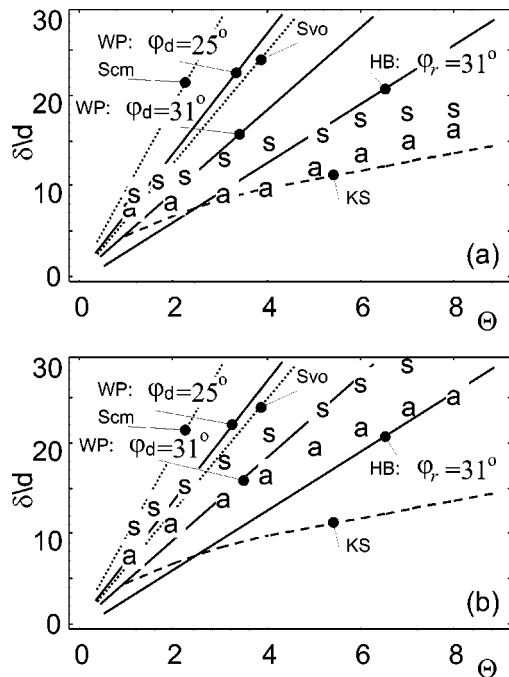


Fig. 10. Stress distribution in stationary conditions. The values are nondimensional with respect to  $\rho_f u_*^2$ ,  $d=0.13$  mm,  $s=2.65$ , and  $\Theta=1.68$



**Fig. 11.** Sheet-flow layer thickness. WP: Wilson and Pugh model; HB: Hanes and Bowen model; KS: Kobayashi and Seo's model. *s* and *a* represent the computed value from the present model for sand and acrylic, respectively; Svo: Sumer et al. from visual observation for Plastic (3.0 and 2.6 mm); Scm: Sumer et al. from concentration measurements for acrylic 0.6 mm. (a) First criterion and (b) second criterion.

The second definition gives higher values of nondimensional thickness and are much closer to the Wilson and Pugh criterion, as shown in Fig. 11(b).

### Velocity Profiles

The fluid velocity profiles shown in Fig. 12 clearly predict a logarithmic region. As a convenient means of interpreting the results of the present model, they have been interpolated using the classical function

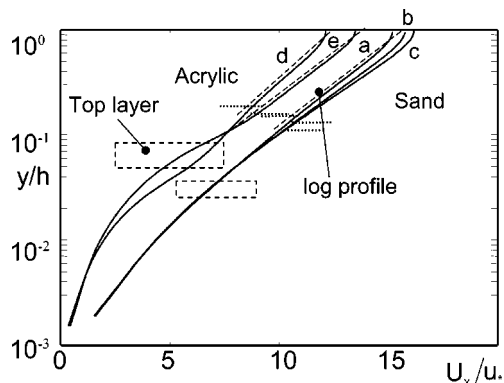


**Fig. 12.** Fluid horizontal velocity, see Table 5 for caption

**Table 5.** Von Kármán's Constant and Reference Level

Material	$\Theta$	$k$	$y_0/d$	$Ri_\delta$	$\alpha$
Sand	1.10	0.3805	1.244	0.015	3.41
Sand	1.68	0.3540	1.528	0.035	3.71
Sand	2.20	0.3322	1.897	0.038	5.37
Acrylic	1.96	0.4534	0.490	—	—
Acrylic	3.99	0.3603	0.959	0.035	3.15

$$U_x = \frac{u_*}{k} \ln\left(\frac{y}{y_0}\right) \quad (36)$$

where the friction velocity is given and the Von Kármán's "constant" is treated as a parameter. The computed values of the constant and of the reference level  $y_0$  are reported in Table 5. The reduction of the Von Kármán's constant with an increase in average concentration is in agreement with many measurements. A detailed analysis of the effects of density stratification (Turner 1973) on the velocity profiles indicates that the Von Kármán's coefficients are corrected according to the expression:

$$k = \frac{k_0}{1 + \alpha Ri_\delta} \quad (37)$$

where  $k_0$ =coefficient without stratification;  $Ri_\delta$ =Richardson number at the top of the shear layer; and  $\alpha$ =coefficient equal to 5 (Webb 1970) nearly equal to the value 4.7 adopted in Businger et al. (1971). The effect is a damping of turbulence. The computed Richardson numbers and correction coefficients are reported in Table 5. The results are in agreement with Pugh and Wilson (1999), with a Richardson number increasing with the Shields parameter and with a more evident damping in turbulence, but the computed correction factor is not constant. The reduction of the Von Kármán's constant is also revealed in duct flows as a second order correction effect on the wall boundary layer (Tennekes and Lumley 1972) and is widely discussed in sediment-laden flows by Lyn (1992).

The Von Kármán's constant is reduced due to the presence of sediments whereas the effective roughness height becomes larger. As a consequence the flow resistance is reduced due to the first effect and is increased to the second effect (see the next section). The second effect is dominant at relatively high volume concentration, as can be deduced observing the friction factor versus the Shield parameter. The increasing of the effective roughness height is addressed to the increased momentum exchange induced by the presence of sediments, similar to the increasing of the effective roughness height due to externally generated turbulence (see Kozakiewicz et al. 1998).

The difference in the velocity profiles for sand and for acrylic is explained in terms of a different importance of the granular phase in the stress balance. The functions  $\chi$  and  $\lambda$  in Eqs. (19) and (21) assume higher values for acrylic than for sand, the dissipation rate in Eq. (22) is lower for acrylic than for sand. The distributions of the pseudotemperature reported in Fig. 9 indicate higher values for acrylic than for sand. The result is that the granular stress is dominant if the dispersed phase is represented by acrylic grains and the fluid phase stress play a minor role. This interpretation is also supported by the turbulence energy distribution reported in Fig. 5.

More interesting is sediment velocity within the sheet flow layer. Pugh and Wilson (1999) report experimental results in which sediment velocity within the sheet flow layer collapses on a straight line. Measurements in the lower half of the layer dis-

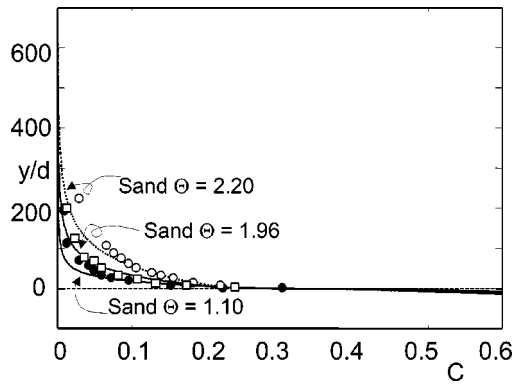


**Fig. 13.** Grain volume concentration for sand; symbols: Sumer et al. and lines: present model

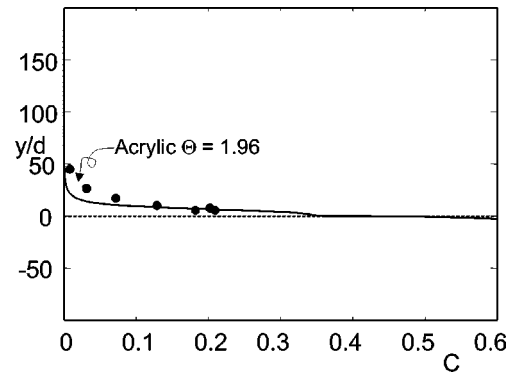


**Fig. 14.** Grain volume concentration for acrylic; symbols: Sumer et al. and lines: present model

played large scattering due to the characteristics of the conductivity probe used in the experiment. The slope of the straight line has an approximate value equal to  $\sim 0.6$ , and the velocity at the top level of the sheet flow layer is  $U_x \cong 9.4u_*$ .

Longo and Lamberti (2002) report experimental results on velocity and pseudotemperature in a dry granular stream (air was the interparticles fluid) in a rotating drum. In the area dominated by collisions the sediment velocity profile is linear; in the area dominated by frictional stress (quasi-static domain) the velocity profile has an inflection.

The sediment velocity profiles computed with the present model, and normalized on the velocity at the top level of the sheet-flow layer (not shown), collapse in a single curve that is not straight, and which possesses a slope equal to  $\sim 0.25-0.35$  at  $y/\delta=1$ . The velocity at the top level of the sheet flow layer is  $U_x \cong 6.8 u_*$  for sand, with higher values being obtained for acrylic. The lag with respect to the horizontal fluid velocity (not shown) is of the order of the friction velocity, being higher for coarse particles, and reaches a minimum immediately outside the sheet-flow layer.

The absence of inflection near the static layer in sediment velocity profiles is presumably due to the poor description of friction. The structure of Eq. (23) is substantially equivalent to a Dirac function and no frictional boundary layer is allowed. Presumably also Pugh and Wilson's data would show inflection of velocity profiles near the static layer if measurements were possible in this area through the impedance probe they used.

Figs. 13 and 14 show predicted concentration profiles versus experimental results for different values of the Shields parameter. The fittings are encouraging, especially for sand grains and the bed load region. When the sediment vertical velocity becomes positive, usually when Shields parameter values are high, an inversion of the concentration profile appears, even though it is limited to two or three grain diameters. This phenomenon is more evident for acrylic grains, as they are lighter than sand grains and therefore subject to strong vertical velocity gradients.

The failure of the model in correctly predicting the behavior of light particles is probably due to the approximate coefficient values adopted in the expression representing interfacial force density. In addition the effects of bursting, detailed in Sumer et al. (1996) but also by Dyer and Soulsby (1988), are not included in the present model. Bursts represent an intermittent convective transport phenomenon, but only diffusion is included in Eq. (12) [see Eq. (14)].

### Transport Rate, Friction Factor

The transport rate can be obtained by integrating in the vertical the sediment horizontal flux. The global transport rate can be divided into bed-load (in the sheet-flow layer) and suspended load

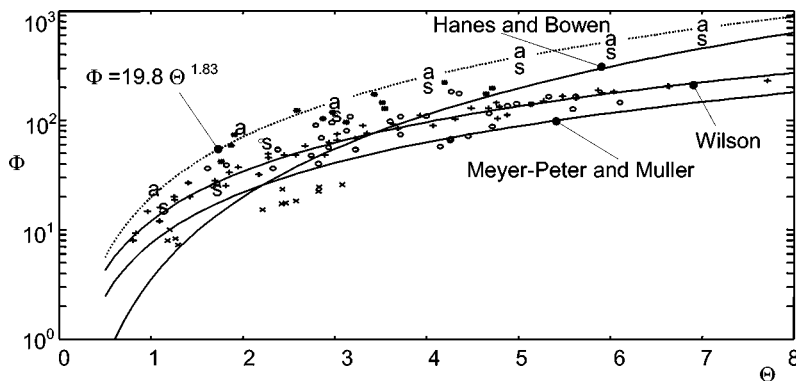


**Fig. 15.** Global nondimensional transport rate versus Shields parameter. Bold lines refer to Hanes and Bowen's model, Wilson's model, and Meyer-Peter and Müller model. Nnadi and Wilson data: +: sand; o, \*: bakelite; and ×: nylon (see Table 2). The dotted line representing the fitting function  $\Phi = 19.8\Theta^{1.83}$  of the computed points for sand (s) and acrylic (a) is also shown.

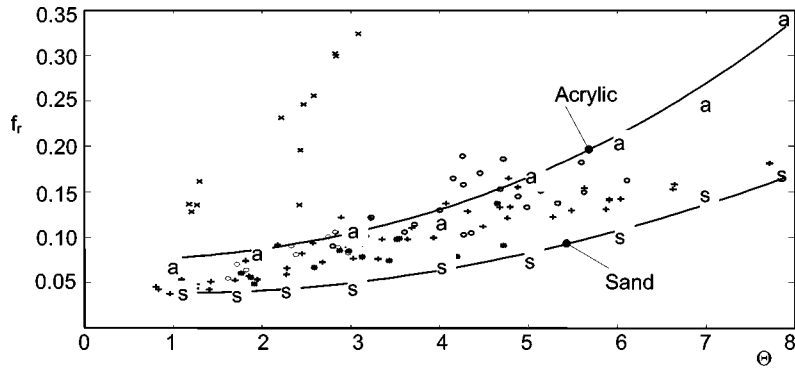


**Fig. 16.** Friction factor versus Shields parameter. The continuous lines refer to the present model applied to sand and acrylic grains as reported in Table 4. Nnadi and Wilson data: +: sand; o, \*: bakelite; and ×: nylon (see Table 3).

$$q_b = \int_0^{\delta} CV_x dy, \quad q_s = \int_{\delta}^h CV_x dy \quad (38)$$

$$\Phi_b = \frac{1.51}{k \tan \varphi_d} \Theta^{3/2} \quad (40)$$

and in nondimensional form may be represented by

$$\Phi_b = \frac{q_b}{\sqrt{g(s-1)d^3}}, \quad \Phi_s = \frac{q_s}{\sqrt{g(s-1)d^3}} \quad (39)$$

A comparison of three different models with the experimental results is shown in Fig. 15. Hanes and Bowen's model, based on the model of Bagnold, is used to describe the grain behavior inside the sheet flow layer. A linear concentration hypothesis, and several assumptions about the movement of grains in the saltating area, address the problem and allow the evaluation of the dynamic friction angle and concentration at the top level of the sheet-flow layer, of its thickness and of the total load. The problem is given in terms of nonlinear coupled equations, whose solution gives a total load that is accurately approximated by the monomial expression  $\Phi_b = 3.5\Theta^{5/2}$ .

Wilson's model is based on a mixing-length approach to describe the dynamics of the fluid; the grains support tangential stress proportional to the concentration, where the fluid shear stress is supposed to vary quadratically in the sheet-flow layer. Assuming a linear concentration profile from the bottom to the top of the sheet-flow layer, the solution gives a transport rate equal to

$k =$  Von Kármán's constant. This result shows little difference with Meyer-Peter and Müller's (1948) semiempirical formula,  $\Phi_b = 8(\Theta - \Theta_c)^{3/2}$ . At high  $\Theta$  values the difference is about 50%.

In the above-mentioned formulas, the Shields parameter is computed on the basis of the effective bottom shear stress due to skin friction. The effective bottom shear stress and the total bottom shear stress coincide for flat bottoms, without any additional resistance due to bed forms.

The results of the present model are given in terms of the total solid discharge (bed load and suspended load), whereas the models of Hanes and Bowen, Wilson and Meyer-Peter, and Müller give results in terms of the bed load. The present model predicts higher transport, especially at higher Shields parameter values. It is consistent with the fact that suspended loads show higher increases in transport, than bed loads, at higher shear rates.

The presence of sediment in suspension and a mobile bed strongly influence the shape of the velocity profile, and the fluid discharge, for a given energy gradient. A global measure of the resistance is obtained as the ratio of the friction velocity, proportional to the stress at the bottom, and the mean fluid velocity. The use of Chezy's formula yields the following expression:

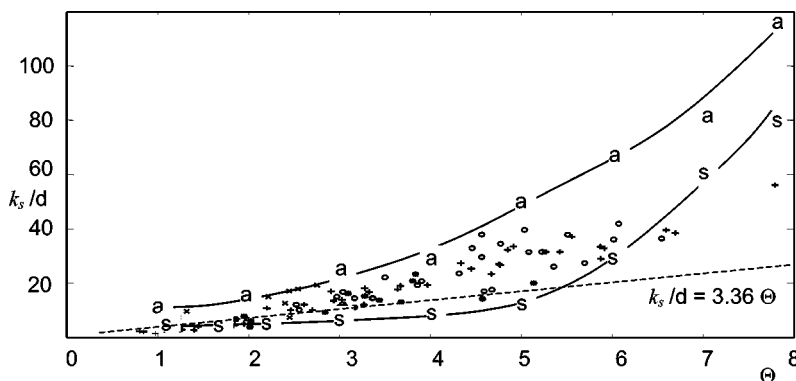


**Fig. 17.** Apparent bed roughness, in number of grain diameters, versus Shields parameter. Wilson's data: +: sand; o, \*: bakelite; and ×: nylon (see Table 3). The straight line is obtained from Pugh and Wilson data (1999).

$$\overline{U}_x = A\sqrt{gRJ} = Au_* \quad (41)$$

where  $\overline{U}_x$ =depth-averaged horizontal fluid velocity;  $A=\overline{U}_x/u_*$ =nondimensional Chezy coefficient;  $R$ =hydraulic radius (computed assuming free surface); and  $J$ =energy gradient. The Darcy Weisbach friction factor, defined as  $f_r=8/A^2=8(u_*/\overline{U}_x)^2$ , has been compared with the experimental results of Nnadi and Wilson, as shown in Fig. 16.

The friction factor increases for higher values of the Shields parameter; the effect is more evident for lighter and coarse particles, as confirmed by experimental results. The apparent roughness of the bed can be evaluated using Colebrook and White's logarithmic formula for fully turbulent motion over a rough plane bed

$$\sqrt{\frac{8}{f_r}} = \frac{1}{k} \ln \left( \frac{12.2R}{k_s} \right) \quad (42)$$

with  $R$  representing the hydraulic radius;  $k$ =reduced Von Kármán's constant (Table 5); and  $k_s=md$  expressing the apparent roughness of the bed in terms of the diameter of the grain. The results are shown in Fig. 17. The apparent roughness varies from 10-grain diameters for a Shields parameter near 1, to  $\sim 100$ -grain diameters for a Shields parameter equal to 8. The value usually assumed for a rough, immobile bed is 2-grain diameters, and is kept independent of the Shields parameter. The straight line forced through the origin is obtained from data reported in Pugh and Wilson (1999). The best fitting line has equation

$$\frac{k_s}{d} = (3.36 \pm 0.49)\Theta \quad (43)$$

The uncertainty in the coefficient represents the standard deviation in the linear estimate. The uncertainty in the experimental data, as Pugh and Wilson (1999) state in their paper, is less than 20% in the bottom stress evaluation (and hence in the Shields parameter if the grain size and the relative density of the sediments are assumed unaffected by errors). Compared to Pugh and Wilson's result, the present model overestimates the apparent roughness at high shear rate. Compared to Wilson's data, the present model bounds most of the experimental points.

## Conclusions

The model outlined in this study, albeit containing simple assumptions concerning the interactions between the fluid and solid phases, appears to correctly reproduce the high concentration layers near the bottom. A region of the domain where the stresses are mainly dispersive in the solid phase is contiguous with a region where the fluid exhibits mainly Reynolds stresses.

The first limitation of the model is the diffusive scheme assumed for the sediment concentration mass balance equation; this scheme works reasonably well at low and moderate concentrations, but fails when the mechanism of transmission of stress becomes mainly collisional, and is inadequate in quasi-static conditions. For future considerations, the proper overlap between the diffusion area and quasi-static area should be defined.

The second limitation is the expression of the interfacial force densities. Such forces have been theoretically and experimentally explored for isolated particles, but to the best of our knowledge few studies have been reported, and no experimental measurements are available for particles at intermediate or high concentrations. In our scheme the interfacial force densities represent the

only direct interaction between the two phases, and a reliable description of these forces is essential in order to obtain a reliable experimental outcome.

The rheology of grains has been modeled with no regard for the interparticles fluid, assuming the symmetry of the stress tensor, and neglecting any kind of clustering of the grains. Such a reductive and limited framework does not reflect the real behavior of the system, as evidenced by numerical simulations (Walton et al. 1991) and experiments. Also friction stress formulation in the granular phase requires improvements.

- A turbulence model for a two-phase system has been applied. The transfer of energy due to correlations between fluid and grain velocity fluctuations is limited to negligible concentrations; no direct mechanism of transfer of energies (turbulence energy and pseudothermal energy) is allowed at intermediate or high grain concentrations. The balance of the different contributions to the dynamics of turbulence highlights the importance of convection in the sheet flow layer.
- The horizontal fluid velocity profiles show a logarithmic behavior in the low concentration area, with the value of the Von Kármán's constant being reduced by the concentration and by density stratification (except for a relatively low Shields parameter and light grains). The lag with respect to the horizontal velocity of grains (not shown) is of the order of the friction velocity, being higher for coarse particles, and reaches a minimum immediately outside the sheet-flow layer.
- The thickness of the sheet-flow layer, defined on the basis of stress distribution, is of the order of 10-grain diameters for  $\Theta=1$ , increasing with the Shields parameter and consistent with the theoretical formulations of Hanes and Bowen (1985) and Wilson and Pugh (1988).
- The global solid discharge, in nondimensional form, increases as a power of the Shields parameter, with values higher than the experimental measurements and forecasts of several other models.
- The friction factor is in reasonable agreement with the experiments; the relationship between global resistance and grain characteristics is best described by expressing the apparent roughness of the bottom in number of grain diameters. The apparent roughness varies from  $\sim 10d$  at  $\Theta=1$ , to higher values for an increasing Shields parameter, with larger values being predicted for acrylic than for sand.

## Acknowledgments

This work was supported by Italian Ministry for Research (MIUR) COFIN 2001 (ex-40%), Parma Research Group, project "Convivere con le frane: Effetti su infrastrutture e insediamenti urbani. Strategie di intervento per la mitigazione del rischio." The numerical model development was undertaken while the writer was a visiting research fellow at HR Wallingford Ltd. (U.K.) and was supported by the European Commission Human Capital Mobility Programme, Contract No. ERBCHBGCT920042. The suggestions of the anonymous reviewers have been greatly appreciated.

## Notation

The following symbols are used in this paper:

- $A$  = Chezy's coefficient;
- $a$  = spatial weighting function;

- $b$  = coefficient;  
 $C$  = sediment phase volume concentration;  
 $C_0$  = maximum sediment phase volume concentration;  
 $C_*$  = critical sediment phase volume concentration;  
 $C_b$  = bottom sediment phase volume concentration;  
 $C_\delta$  = sediment phase volume concentration at the top of the sheet flow layer;  
 $C_D, C_M, C_P, C_L$   
 = drag, added mass, pressure, and lift coefficients for a single sphere;  
 $C_{De}, C_{Me}, C_{Le}$   
 = effective drag, mass, and lift coefficients for a cloud of spheres;  
 $C_\mu, C_{\varepsilon 1}, C_{\varepsilon 2}, C_{\varepsilon 3}, C_{C5}$   
 = coefficients in the  $\kappa$ - $\varepsilon$  model;  
 $\mathbf{D}_f$  = rate of deformation tensor for the fluid;  
 $D$  = pseudothermal energy dissipation rate due to the particle-boundary collision, diffusion;  
 $D_s, D_f$  = symbols for material derivative respect to sediments, fluids;  
 $d$  = grain diameter;  
 $d_{50}$  = grain diameter having a frequency of 50% in the frequency distribution of the mixture;  
 $e, e_w$  = elastic energy restitution coefficients in the domain and near the wall;  
 $\mathbf{f}$  = force per unit mass;  
 $f$  = function;  
 $f_r$  = friction factor;  
 $f_1, f_{11}, f_2, f_3, f_4, f_5$   
 = functions in the model of Lun et al. (1984);  
 $f_{xst}, f_{yst}$  = drag components;  
 $F_{stat}$  = term in the stationary drag;  
 $FS$  = coefficient in the expression of the frictional stresses;  
 $g$  = acceleration of gravity;  
 $h$  = height of the domain;  
 $I$  = pseudothermal energy dissipation rate;  
 $J$  = energy gradient;  
 $k$  = Von Kármán's constant;  
 $k_s$  = apparent roughness of the bottom;  
 $l$  = turbulence length scale;  
 $\mathbf{M}_j, \mathbf{M}_s^d, \mathbf{M}_f^d$   
 = interfacial force densities;  
 $M_{sx}^d, M_{sy}^d$  = interaction force density components;  
 $m$  = coefficient;  
 $\mathbf{n}$  = unit normal;  
 $n$  = number of particles per unit volume;  
 $P$  = production of turbulent kinetic energy;  
 $P_{extra}$  = extra production of turbulent kinetic energy;  
 $P_s, P_f$  = isotropic component of the sediment and fluid phase stress tensor;  
 $p_{int}$  = pressure at the interface;  
 $q_b$  = bed load solid discharge;  
 $q_s$  = suspended load solid discharge;  
 $\mathbf{q}_{PT}$  = pseudothermal energy flux;  
 $q_{PTy}$  = vertical component of the pseudothermal energy flux;  
 $R$  = hydraulic radius;  
 $\mathbf{s}$  = space vector;  
 $s$  = density of the sediment phase relative to the fluid phase;  
 $\mathbf{T}$  = stress tensor;  
 $T$  = granular pseudotemperature;
- $T_b$  = pseudotemperature at the bottom;  
 $t$  = time;  
 $\mathbf{T}_s, \mathbf{T}_f$  = stress tensor for sediments, fluid;  
 $T_{ij}=ij$  = component of  $\mathbf{T}$ ;  
 $\mathbf{U}$  = velocity vector;  
 $\mathbf{U}_f, \mathbf{V}_s$  = velocity vector of the fluid and sediment phase;  
 $\mathbf{U}_i$  = velocity vector of the interface;  
 $\mathbf{U}'$  = fluctuation of velocity vector;  
 $U$  = imposed external velocity oscillation;  
 $U'$  = velocity scale;  
 $U'_i$  = fluctuation of velocity  $i$  component;  
 $U_x, V_x, U_y, V_y$   
 = velocity components along  $x$  and  $y$  direction for the fluid and sediments;  
 $u_{seep}$  = seepage fluid velocity;  
 $u_*$  = frictional velocity related to the fluid tangential stress;  
 $w$  = grains settling velocity, velocity scale;  
 $X_j$  = generalized function;  
 $x, y$  = space independent variables;  
 $y_b, y_t$  = bottom and top spatial coordinate;  
 $y_0$  = reference level;  
 $\alpha$  = bed slope angle, coefficient;  
 $\beta_1, \beta_2$  = coefficients;  
 $\delta$  = thickness of the sheet-flow layer;  
 $\delta_{ij}$  = Kronecker operator;  
 $\varepsilon$  = turbulence energy dissipation rate;  
 $\varepsilon_{extra}$  = extra dissipation rate of turbulent energy;  
 $\eta$  = free surface slope;  
 $\Theta$  = Shields parameter;  
 $\Theta_c$  = critical Shields parameter;  
 $\kappa$  = turbulence kinetic energy;  
 $\lambda$  = function in the pseudothermal energy balance for the granular phase;  
 $\lambda_f, \lambda_s$  = fluid and sediment bulk viscosities;  
 $\mu_f, \mu_s$  = fluid and sediments shear viscosities;  
 $\nu$  = molecular fluid viscosity;  
 $\nu_t$  = turbulent eddy diffusivity;  
 $\nu_s$  = sediment diffusivity;  
 $\rho$  = mass density;  
 $\tau_s, \tau_f$  = components of the stress tensor for the sediment phase and fluid phase;  
 $\tau_{sk}, \tau_{sc}, \sigma_{sk}, \sigma_{sc}$   
 = kinetic and collisional tangential and normal stresses for the sediment phase;  
 $\tau_{fric}, \sigma_{fric}$  = tangential and normal frictional stresses in the sediment phase;  
 $\Phi_j$  = spatial weighted average of the phasic function  $X_j$ ;  
 $\Phi_b$  = nondimensional bed load solid discharge;  
 $\Phi_s$  = nondimensional suspended load solid discharge;  
 $\varphi_s, \varphi_d$  = static and dynamic internal friction angle for the granular system;  
 $\varphi'$  = Coulombic friction angle for the granular system;  
 $\chi$  = function in the stress tensor of the granular phase; and  
 $\Omega$  = fluid phase vorticity.
- Symbols**  
 $\langle \dots \rangle$  = weighted spatial average operator;  
 $\sim$   
 $(\dots)$  = phasic space average operator;

- $(\overline{\dots})$  = density weighted average operator;  
 $(\overline{\dots})'$  = time fluctuating component; and  
 $(\overline{\overline{\dots}})$  = time averaged component.

## References

- Ahilan, R. V., and Sleath, J. F. A. (1987). "Sediment transport in oscillatory flow over flat beds." *J. Hydraul. Eng.*, 113(3), 308–322.
- Anderson, K. G., and Jackson, R. J. (1992). "A comparison of the solutions of some proposed equations of motion of granular materials for fully developed flow down inclined planes." *J. Fluid Mech.*, 241, 145–168.
- Bagnold, R. A. (1954). "Experiments on a gravity-free dispersion of large solid spheres in a Newtonian fluid under shear." *Proc. R. Soc. London, Ser. A*, 225, 49–63.
- Brørs, B. (1991). "Turbidity current modelling." PhD thesis, The University of Trondheim, Norway.
- Businger, J. A., Wyngaard, J. C., Izumi, Y., and Bradley, E. F. (1971). "Flux profile relationships in the atmospheric surface layer." *J. Atmos. Sci.*, 28, 181–189.
- Chapman, S., and Cowling, T. G. (1970). *The mathematical theory of non-uniform gases*, 3rd Ed., Cambridge University Press, Cambridge, U.K., 423+xxiv.
- Chen, C. L., and Ling, C. H. (1996). "Granular-flow rheology: Role of shear-rate number in transition regime." *J. Eng. Mech.* 122(5), 469–480.
- Chen, C. L., and Ling, C. H. (1998). "Rheological equations in asymptotic regimes of granular flow." *J. Eng. Mech.* 124(3), 301–310.
- Dong, P., and Zhang, K. (1999). "Two-phase flow modelling of sediment motions in oscillatory sheet flow." *Coastal Eng.*, 36, 87–109.
- Drew, D. A. (1983). "Mathematical modeling of two-phase flow." *Annu. Rev. Fluid Mech.* 15, 261–291.
- Dyer, K. R., and Soulsby, R. L. (1988). "Sand transport on the continental shelf." *Annu. Rev. Fluid Mech.* 20, 295–324.
- Elghobashi, S. E., and Abou-Arab, T. W. (1983). "A two-equation turbulence model for two-phase flows." *Phys. Fluids* 26(4), 931–938.
- Gutt, G. M., and Haff, P. K. (1991). "Boundary conditions on continuum theories of granular flow." *Int. J. Multiphase Flow*, 17(5), 621–634.
- Haff, P. K. (1983). "Grain flow as a fluid-mechanical phenomenon." *J. Fluid Mech.*, 134, 401–430.
- Hanes, D. M., and Bowen, A. J. (1985). "A granular-fluid model for steady intense bed-load transport." *J. Geophys. Res.*, 90(C5), 9149–9158.
- Hui, K., Haff, P. K., Ungar, J. E., and Jackson, R. (1984). "Boundary conditions for high-shear grain flows." *J. Fluid Mech.*, 145, 223–233.
- Hunt, M. L., Zenit, R., Campbell, C. S., and Brennen, C. E. (2002). "Revisiting the 1954 suspension experiments of R. A. Bagnold." *J. Fluid Mech.* 452, 1–24.
- Jenkins, J. T., and Askari, E. (1991). "Boundary conditions for rapid granular flows: Phase interfaces." *J. Fluid Mech.*, 223, 497–508.
- Jenkins, J. T., and Richman, M. W. (1986). "Boundary conditions for plane flows of smooth, nearly elastic, circular disks." *J. Fluid Mech.*, 171, 53–69.
- Johnson, P. C., and Jackson, R. (1987). "Frictional-collisional constitutive relations for granular materials, with application to plane shearing." *J. Fluid Mech.*, 176, 67–93.
- Johnson, P. C., Nott, P., and Jackson, R. (1990). "Frictional-collisional equations of motion for particulate flows and their application to chutes." *J. Fluid Mech.*, 210, 501–535.
- Kenning, V. M., and Crowe, C. T. (1997). "On the effects of particles on carrier phase turbulence in gas-particle flows." *Int. J. Multiphase Flow* 23, 403–408.
- Kobayashi, N., and Seo, S. N. (1985). "Fluid and sediment interaction over a plane bed." *J. Hydraul. Eng.*, 111(6), 903–921.
- Kozakiewicz, A., Sumer, B. M., Fredsøe, J., Deigaard, R., and Cheng, N.-S. (1998). "Effect of externally generated turbulence on wave boundary layer." Progress Rep. ISVA, No. 77, Technical University of Denmark.
- Lamberti, A., Montefusco, L., and Valiani, A. (1991). "A granular-fluid model of the stress transfer from the fluid to the bed." *Sand transport in rivers, estuaries and the sea*, R. L. Soulsby and R. Bettes, eds., Balkema, Rotterdam.
- Longo, S., and Lamberti, A. (2002). "Grain shear flow in a rotating drum." *Exp. Fluids* 32, 313–325.
- Lun, C. K. K., Savage, S. B., Jeffrey, D. J., and Chepurmy, N. (1984). "Kinetic theories for granular flow: Inelastic particles in Couette flow and slightly inelastic particles in a general flowfield." *J. Fluid Mech.*, 140, 223–256.
- Lyn, D. A. (1992). "Turbulence characteristics of sediment-laden flows in open channel." *J. Hydraul. Eng.*, 118(7), 971–988.
- Maude, A. D., and Withmore, R. L. (1958). "A generalised theory of sedimentation." *Br. J. Appl. Phys.*, 7(12), 58–71.
- Meyer-Peter, E., and Müller, R. (1948). "Formulas for bed-load transport." *Rep. 2nd Meet. Int. Assoc. Hydraul. Struct. Res.*, Stockholm, 39–64.
- Mokeyev, Y. G. (1977). "Effect of particle concentration on their drag and induced mass." *Fluid Mech.-Sov. Res.*, 6, 161–180.
- Nnadi, F. N., and Wilson, K. C. (1992). "Motion of contact-load particles at high shear stress." *J. Hydraul. Eng.*, 118(12), 1670–1684.
- Nott, P., and Jackson, R. (1992). "Frictional-collisional equation of motion for granular materials and their application to flow in aerated chutes." *J. Fluid Mech.*, 241, 124–144.
- Pasquarell, G. C., and Ackermann, N. L. (1989). "Boundary conditions for planar granular flows." *J. Eng. Mech.*, 115(6), 322–327.
- Pugh, F. J., and Wilson, K. C. (1999). "Velocity and concentration distributions in sheet flow above plane beds." *J. Hydraul. Eng.* 125(2), 117–125.
- Ribberink, J. S., and Al-Salem, A. A. (1995). "Sheet flow and suspension of sand in oscillatory boundary layers." *Coastal Eng.*, 25, 1283–1302.
- Rotta, J. C. (1951). "Statistische theorie nichthomogener turbulenz." *Z. Phys.*, 129, 547–570.
- Rubey, W. (1933). "Settling velocities of gravel, sand and silt particles." *Am. J. Sci.*, 225, 323–345.
- Sumer, B. M., Kozakiewicz, A., Fredsøe, J., and Deigaard, R. (1996). "Velocity and concentration profiles in sheet-flow layer of movable bed." *J. Hydraul. Eng.* 122(10), 549–558.
- Tchen, C.-M. (1947). "Mean value and correlation problems connected with the motion of small particles suspended in a turbulent fluid." dissertation, Delft, The Netherlands.
- Tennekes, H., and Lumley, J. L. (1972). *A first course in turbulence*, The MIT Press, Cambridge, Mass. 300 + xii.
- Turner, J. S. (1973). *Buoyancy effects in fluids*, Cambridge University Press, London.
- Walton, O. R., Kim, H., and Rosato, A. D. (1991). "Microstructure and stress differences in shearing flows." *Mechanics computing in 1990s and beyond*, H. Adeli and K. Sierakowski, eds., 1249–1253.
- Webb, E. K. (1970). "Profile relationships: The log-linear range, and the extension to strong stability." *Q. J. R. Meteorol. Soc.*, 96, 67–90.
- Wilson, K. C. (1987). "Analysis of bed load motion at high shear stress." *J. Hydraul. Eng.*, 113(1), 97–103.
- Wilson, K. C., and Pugh, F. J. (1988). "Dispersive force modelling of turbulent suspension in heterogeneous slurry flow." *Can. J. Chem. Eng.*, 66, 721–727.